JOURNAL OF MATERIALS SCIENCE 12 (1977) 1587–1597

Wedge crack nucleation in Type 316 stainless steel

D. G. MORRIS, D. R. HARRIES
Metallurgy Division, AERE, Harwell, Didcot, Oxfordshire, UK

Type 316 austenitic steel has been heat-treated to produce a range of grain sizes and then creep-tested at 625° C at various stresses so as to examine the nucleation and the factors which effect the nucleation of grain-boundary triple point or "wedge" cracks. An internal marker technique was used to evaluate the extent of the grain-boundary sliding in relation to the total creep strain. Triple point crack nucleation occurred over the entire range of grain sizes and stresses examined when the product of the stress and grain-boundary displacement reached a critical value; the effective surface energy for grain boundary fracture, estimated using an expression derived by Stroh, was in approximate agreement with the surface free energy value indicating that only limited relaxation occurred by plastic deformation. The first cracks were observed to form along grain boundary facets perpendicular to the applied stress direction and with the sliding grain boundaries at high angles (60 to 80°) to the crack growth direction. Subsequent cracking occurred under conditions which deviated slightly from this initial condition, and the increase in crack density with strain was expressed in terms of geometrical factors which take account of the orientation effects.

1. Introduction

The nucleation of grain-boundary creep damage, both in the form of triple point or "wedge" cracks and cavities has been studied extensively (see, for example, the recent review by Greenwood [1]). In general, the nucleation of wedge cracks has been treated as analogous to cleavage crack formation in brittle solids [2–4] by considering the stress concentrations produced at grain-boundary triple points by grain-boundary sliding. The application of such theories to wedge crack nucleation during creep is of dubious value, since it is difficult to imagine how the high stress required to cause grain-boundary de-cohesion may be produced when deformation mechanisms capable of allowing stress relaxation are operating. A more realistic model of crack nucleation must consider the relative time dependencies of the mechanisms involved, both stress-concentration and stress-relaxation mechanisms. The balance between such mechanisms will determine whether crack nucleation is feasible, and will also reflect the extent of work required to create a crack. In the absence of relaxation mechanisms brittle-crack models such as that of Stroh [3] will apply, and the following conditions of crack nucleation will hold:

$$\sigma_s^2 = \frac{3\pi\gamma G}{8(1-\nu)d} \quad (1)$$

$$\sigma_s nb = \frac{3\pi^2}{8}\gamma \quad (2)$$

where σ_s is the shear stress on the sliding boundary, γ the effective surface energy per unit of fracture surface, G the shear modulus, d the grain size, nb the slip displacement and ν the Poisson's Ratio.

When relaxation mechanisms operate, crack nucleation is more difficult and nucleation criteria will contain time-dependent terms. Use of the above expressions to describe nucleation is incorrect, and this is reflected in an increase in the effective fracture surface energy.

Good agreement between experimental observations and predictions based on the Stroh model

has been found when considering the stress required to produce triple point cracks in materials of different grain sizes [5, 6], but relatively little other work has been carried out to examine the details of the nucleation process. The classification of the large-scale damage in this way is ambiguous in that the grain-boundary damage observed may be determined by details of the growth mechanism rather than by the mechanism of nucleation [7]; for example, cavities nucleated on grain boundaries may grow and have the same appearance as triple point cracks. It is thus essential to examine damage nucleation in its early stages to avoid such confusion. The present study is concerned with the nucleation of grain-boundary damage at applied stresses sufficient to nucleate triple point cracking in Type 316 austenitic steel; that is Equation 1 is satisfied for each grain size examined. The nucleation process has been examined both to determine the extent to which a Stroh-type brittle model may apply to a situation where considerable ductility is involved and where extensive relaxation of stress concentrations occurs, and also in an attempt to quantify the various parameters involved and their effects on crack density.

2. Experimental procedure

The composition of the Type 316 steel used is given in Table I. Circular cross-section creep-rupture specimens with a 12 mm gauge length and 6 mm diameter were machined from bar and a series of grain sizes produced by annealing specimens in sealed silica tubes at temperatures in the range 1050 to 1350° C, terminating with a quench into water. All annealing treatments at temperatures above 1050° C were followed by a further anneal for 30 min at 1050° C and a water quench, such that a standard solution treatment was given to the specimens. The smallest grain size was achieved by straining the specimens 25% in tension prior to annealing for 20 min at 1050° C.

TABLE I Analysis of Type 316 steel

Element	wt %
C	0.052
Si	0.70
Mn	1.08
Cr	16.86
Ni	11.32
Mo	2.09
S	0.009
P	0.028
B	0.003

The creep-rupture testing was carried out in air using Dennision lever machines at constant load and a temperature of 625° C. The majority of the tests was made at an initial stress of 220 MN m^{-2}, with a limited number at 200, 290 and 330 MN m^{-2}. Some of the specimens were crept to predetermined strain levels and the gauge lengths examined metallographically.

Necking occurred prior to specimen failure so that there was considerable variation of strain and crack density along the gauge length. The experimental values of creep strain and crack density quoted here refer to those associated with the neck of the specimen. The neck strain was determined by measuring the neck diameter and an equivalent neck strain calculated as $(A_0/A - 1)$ where A_0 and A refer to the initial and final cross-sectional areas. The strain value is equivalent to the longitudinal strain of the neck element, and is equivalent to the specimen longitudinal strain where there is no necking.

Longitudinal sections of the gauge portions of the specimens were carefully prepared for optical microscope examination by conventional grinding techniques and by polishing on pads containing diamond paste. Polishing on 1 μm diamond paste was followed by a light etch using 20% sulphuric acid and the polish-etch procedure repeated six times to ensure that all cracks were revealed. The specimens containing very few cracks were examined at high magnification to enable the cracks to be distinguished from other grain boundary features. A scanning electron microscope with an EDAX attachment was also used to examine the grain-boundary cracks and particles formed during creep.

The extents of the grain-boundary sliding were estimated only in specimens crept to failure by measuring the transverse displacements of stringered inclusions which crossed grain boundaries. In each case the transverse displacement w, and the angle ϕ, between the line of inclusions and the grain boundary were recorded; the mean displacement parallel to the applied stress direction is then given by [8]:

$$\bar{u} = 2\overline{\left(\frac{w}{\tan\phi}\right)} \tag{3}$$

The amount of grain boundary strain was calculated as:

$$\epsilon_{gbf} = \bar{u}/l \tag{4}$$

TABLE II Treatments given to produce variations in grain size.

Annealing treatment*	Grain size (μm)
25% Prestrain and 20 min at 1050° C	25
45 min at 1050° C	50
45 min at 1150° C	85
$1\frac{1}{2}$ h at 1250° C	175
1 h at 1350° C	450

*All treatments above 1050° C were followed by an anneal of 30 min at 1050° C.

where l is the grain diameter and ϵ_{gbf} is the grain boundary strain at fracture.

Although relatively large displacements were measured on fractured specimens, the number of offsets which could be examined was limited and the average results are therefore subject to large standard deviations (estimated to be approximately ± 25%).

3. Experimental results

3.1. Grain sizes

The initial treatments and mean grain diameters of the specimens are listed in Table II; the grain sizes vary by a factor of 18 from 25 to 450 x 10^{-6} m.

3.2. Creep-rupture data

The creep-rupture results for the specimens tested at 220 MN m^{-2} are shown in Figs. 1 and 2. Both the strain on loading and the minimum creep rate increased with increasing grain size. A similar increase in minimum creep rate with increasing grain sizes was obtained by Garofalo *et al.* [9] in an austenitic iron-based alloy with large grain sizes; however, these authors also observed an increase in minimum creep rate on decreasing the grain size below about 50 μm, and this effect was not apparent in the present work. The rupture lives and ductilities were clearly related, a decrease in rupture strain being associated with a decrease in rupture life, but it is obvious that other factors were involved.

The rupture lives and strains of specimens with a mean grain diameter of 50 μm tested at 200, 290 and 330 MN m^{-2} were 700 h and 70%, 12 h and 50% and 4 h and 60% respectively.

3.3. Grain-boundary sliding data

A typical micrograph illustrating the transverse displacement of a line of inclusions due to grain boundary sliding is shown in Fig. 3. The values of $\bar{u}$, ϵ_{gbf} and γ^* (the ratio of grain-boundary strain

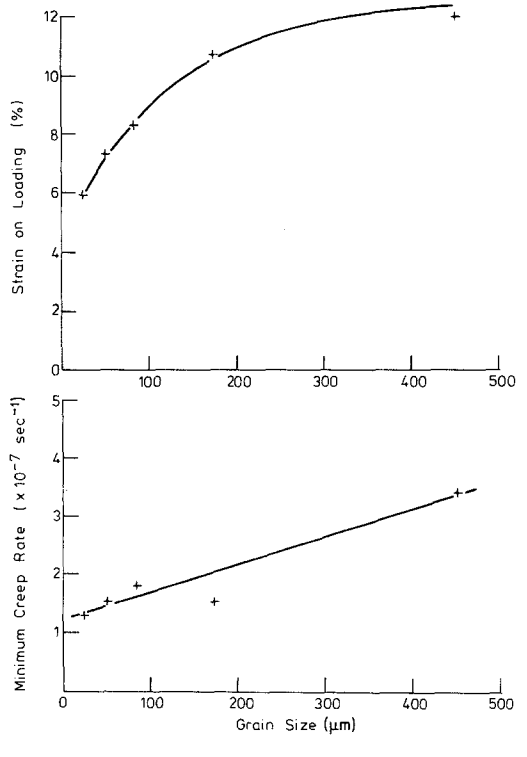

Figure 1 Strain on loading and minimum creep rate as a function of grain size for Type 316 steel at 220 MN m^{-2} and 625° C.

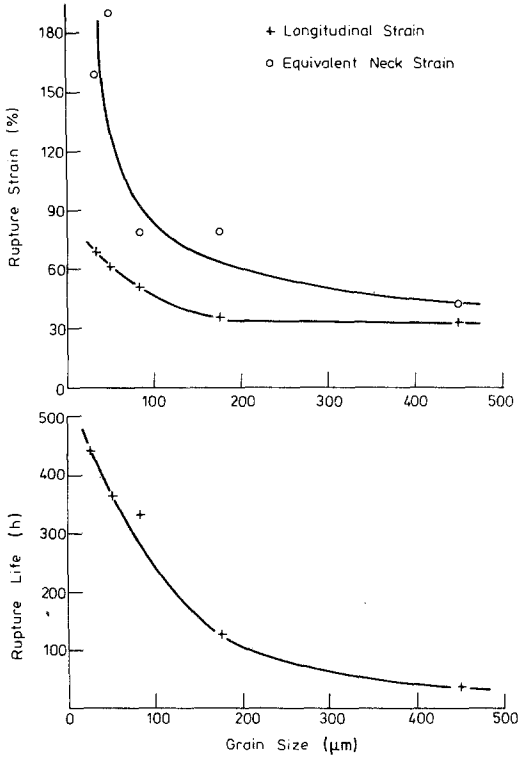

Figure 2 Rupture strain and rupture life as a function of grain size at 220 MN m^{-2} and 625° C.

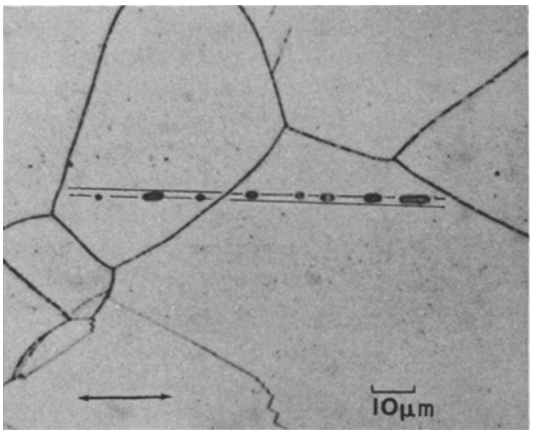

Figure 3 Micrograph illustrating displacement of inclusion line at grain boundary. The direction of applied stress is indicated by arrow.

to total strain) are plotted as a function of grain size in Fig. 4. All three parameters decreased with increasing grain size, with the exception that $\bar{u}$ remained sensibly constant at the larger grain sizes.

3.4. Metallographic observations

Wedge cracks, nucleated at grain boundary triple points, were the only type of boundary damage detected at relatively low strains; at higher strains a few cracks also nucleated at grain boundary/twin boundary junctions. In general, the cracks propagated along the boundaries almost normal to the applied stress direction and terminated on reaching the other ends of the facets, see Fig. 5. At higher strain levels, and correspondingly larger crack densities, the cracks were again oriented predominantly normal to the stress direction but there was an increased range of crack orientations, see Figs. 5 and 6. The angle θ between the wedging grain boundaries, at the open end of the crack, was about 140 to 160° for the first cracks to nucleate whereas at higher crack densities the angular range was much wider, with the distribution peaking at 100 to 170° (illustrated in Figs. 5 and 6 for grain sizes of 50 and 175 μm). Extensive grain-boundary reorientation occurred during the creep tests (see Fig. 5b) and the orientation distributions corresponding to high strains in part reflected this change. Nevertheless, close examination of the distribution plots and the orientations of small cracks (i.e. presumably just nucleated) suggests that the range of orientations corresponding to nucleation was increased at high strains.

The unambiguous determination of crack density was complicated by the presence of large intergranular particles which superficially exhibited many similar features to the cracks; see Fig. 7. Particles ranging in length up to 50 μm were only detected in the strained gauge lengths and were not evident in the unstrained heads of the creep-

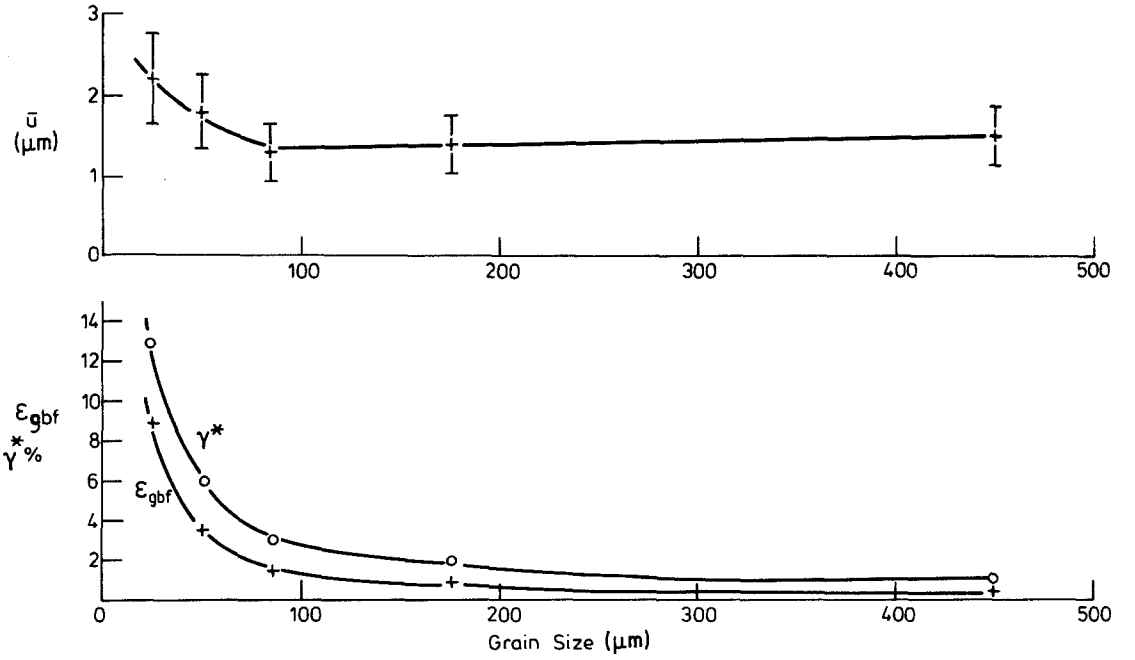

Figure 4 Grain-boundary displacement $\bar{u}$, grain-boundary strain at failure ϵ_{gbf} and the ratio of grain-boundary strain to total strain as a function of grain size.

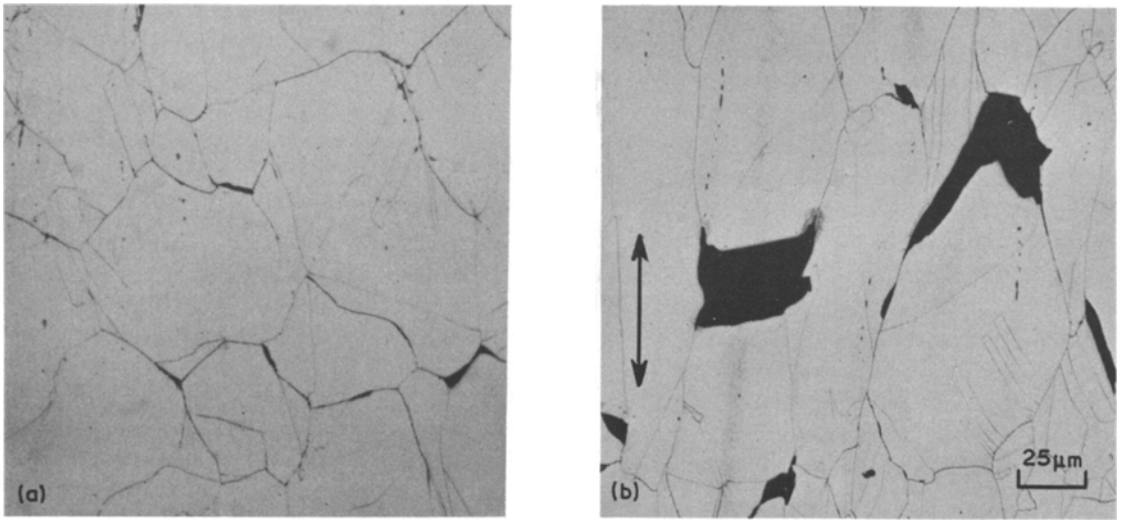

Figure 5 Typical wedge crack distribution (a) after straining 70% (b) after fracture, strain $\simeq$180%. Grain size 50 μm. The direction of applied stress is indicated by the arrow.

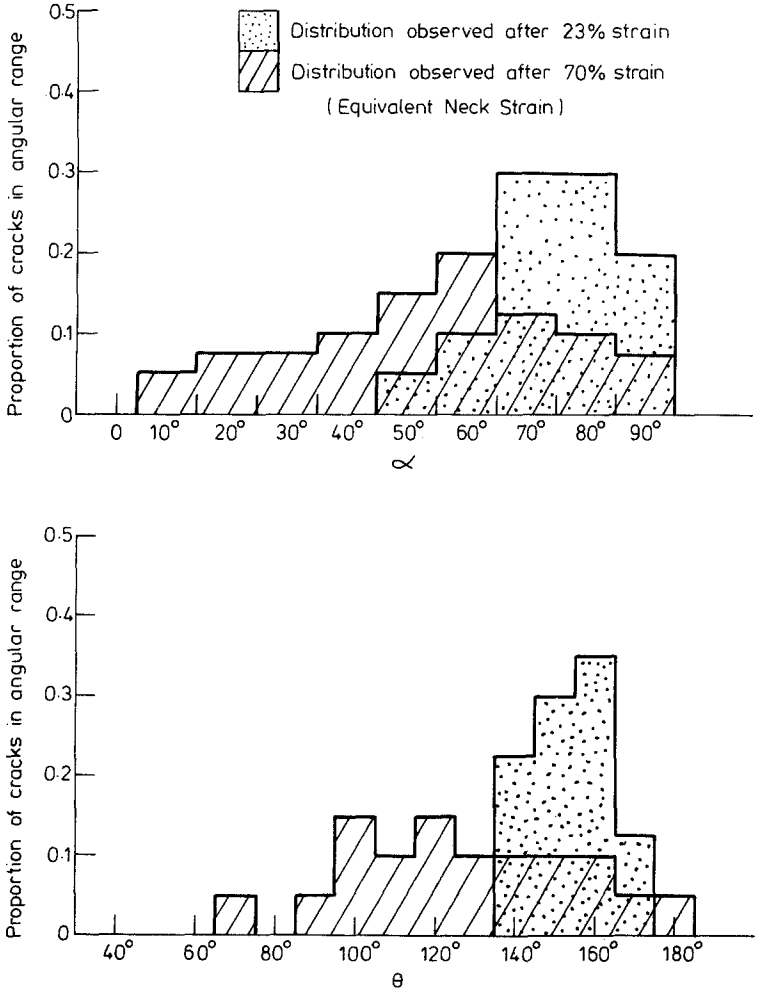

Figure 6 Orientation distribution of crack plane (α) and angular distribution of wedging grain boundaries (θ). Grain size 175 μm.

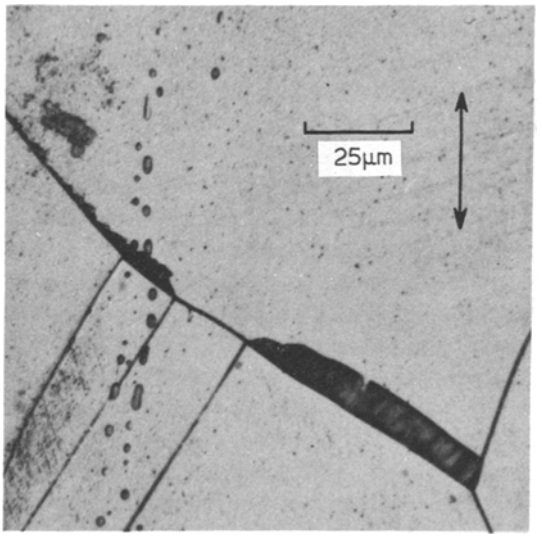

Figure 7 A massive grain boundary particle observed in a specimen of grain size 85 μm after creeping for 65 h at 220 MN m^{-2} and 625° C. The direction of applied stress is indicated.

rupture tested specimens. The particles were randomly oriented and this observation, together with the ability to focus down into cracks, was used in distinguishing between wedge cracks and particles. The identity of these particles has subsequently been determined and will be reported at a later date.

3.5. Crack nucleation

The wedge cracks nucleated at a strain of 16 to 18% for all grain sizes as indicated in Fig. 8 at 220 MN m^{-2}. At this stage, the specimen strains were uniform so that the equivalent neck strains and measured longitudinal strains were similar. The cracks were uniformly distributed and hence the mean crack density was determined over the entire section area. The density of cracks increased rapidly for intermediate strain levels and necking occurred at strains greater than about 30% for each grain size. At strains greater than 30 to 40% there was only a relatively small increase in crack density and the plot of log crack density versus equivalent neck strain appeared to approach saturation. The crack density at which saturation was approached increased with decreasing grain size; see Fig. 9. Fig. 10 shows that the saturation level of crack density per grain (expressed as the ratio of number of cracks per unit area to the number of grains per unit area) was approximately the same for each grain size examined.

The effect of applied stress on the crack density of the steel specimens with a grain size of 50 μm is illustrated in Fig. 11. It appears that the crack density at a given strain was reduced at the higher stresses and it is possible that nucleation of cracks at higher stresses did not occur until strains in

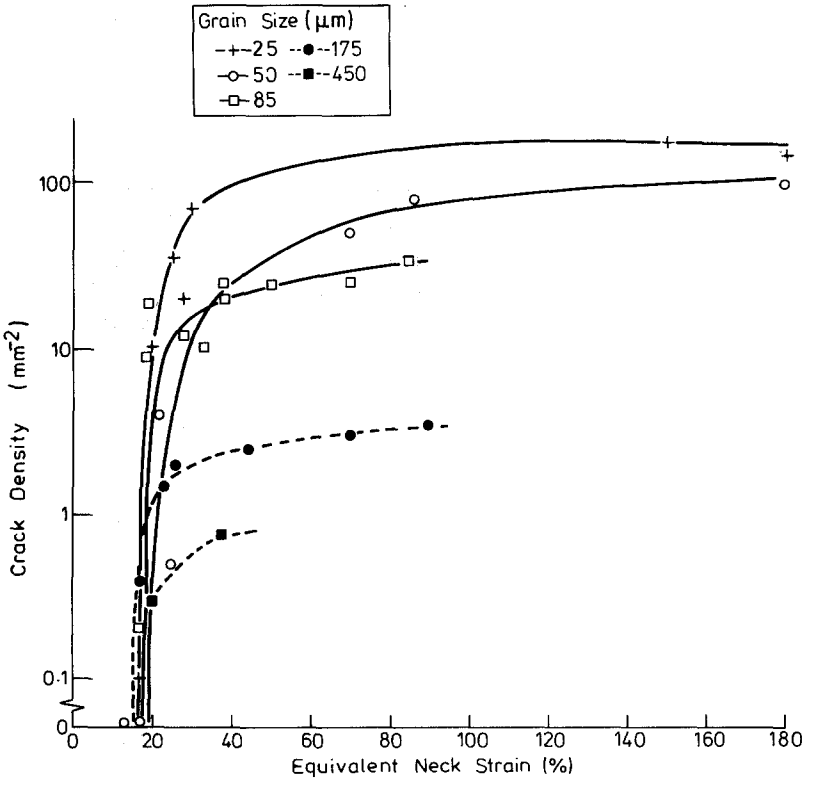

Figure 8 Crack density (mm^{-2}) as a function of equivalent neck strain for each of the grain sizes examined. Specimens tested at 220 MN m^{-2}.

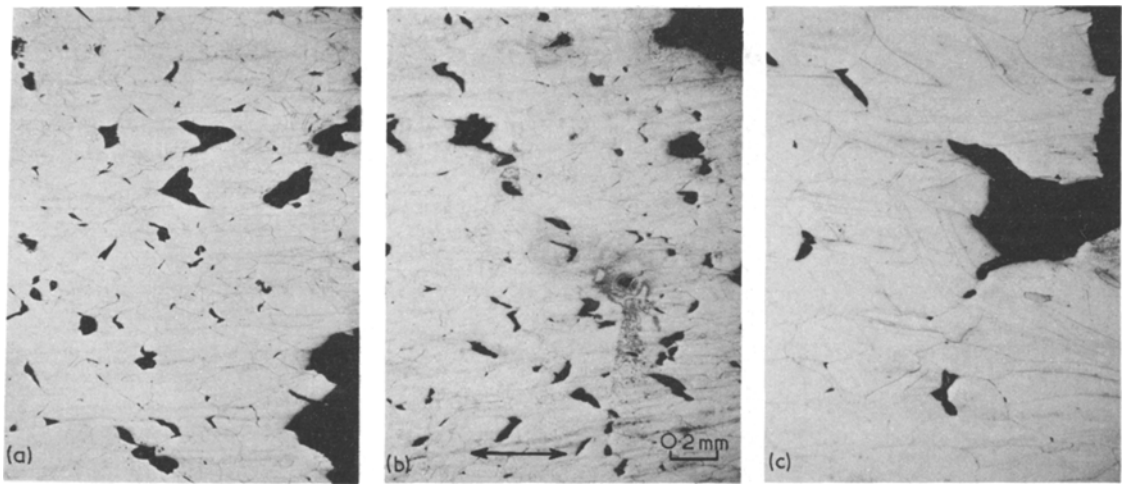

Figure 9 Micrographs illustrating variation of crack density at fracture with grain size. Grain size (a) 50 μm (b) 85 μm (c) 175 μm. Direction of applied stress indicated.

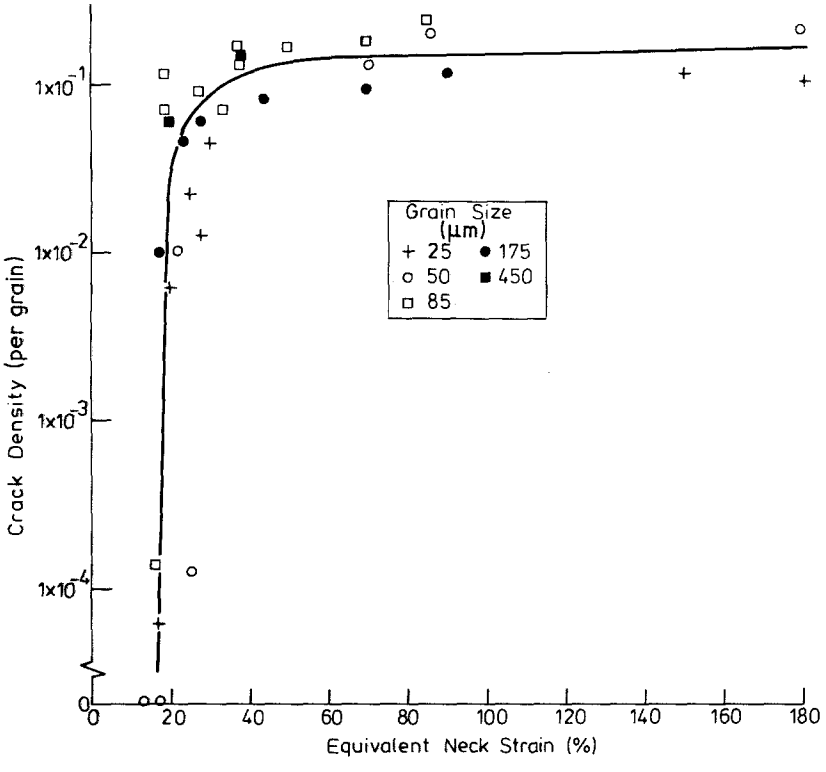

Figure 10 Crack density (number/grain) as a function of equivalent neck strain for each of the grain sizes examined. Tested at 220 MN m^{-2}.

excess of about 35% were achieved. Crack nucleation at 200 MN m^{-2} occurred at the same strain as at 220 MN m^{-2}, namely 16 to 18%.

4. Discussion

4.1. Grain-boundary sliding

Despite the large scatter in experimental results the ratio of grain boundary to total strain (γ^*) determined for a grain size of 85 μm agrees very well with the value determined by Garofalo *et al.* [10] for a Type 316 stainless steel having a grain size of 90 μm, tested at a stress level of 220 MN m^{-2}. In evaluating the influence of grain size on grain boundary sliding, it is necessary in the present case to consider γ^* since the experimental values of both $\bar{u}$ and ϵ_{gbf} determined here depend on the rupture ductility. The variation in γ^* is consistent with grain boundary strain being inversely proportional to the grain diameter, see Fig. 12, in agreement with the relationship proposed by

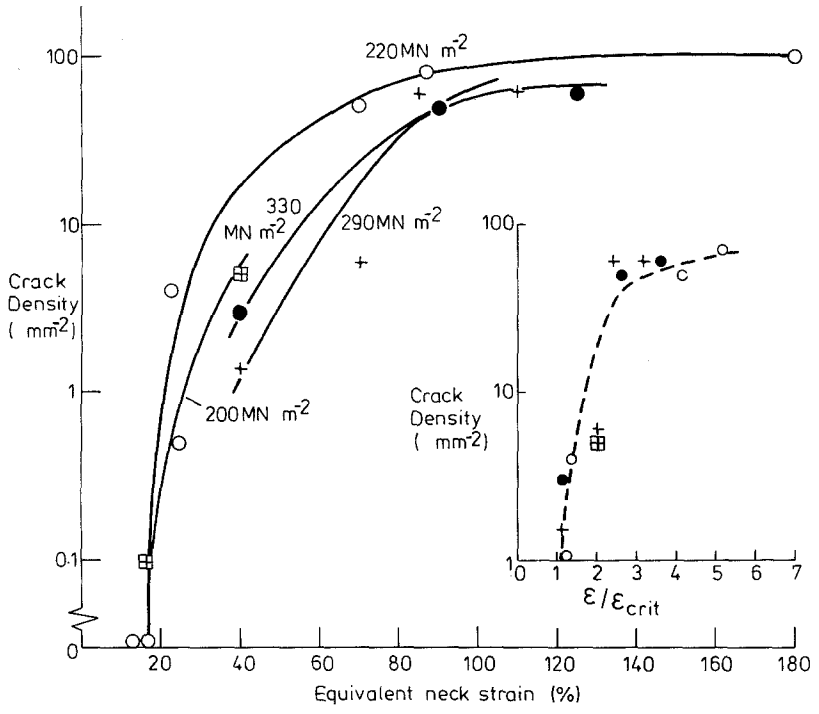

Figure 11 Crack density (mm^{-2}) as a function of equivalent neck strain for several creep stresses. Grain size 50 μm.

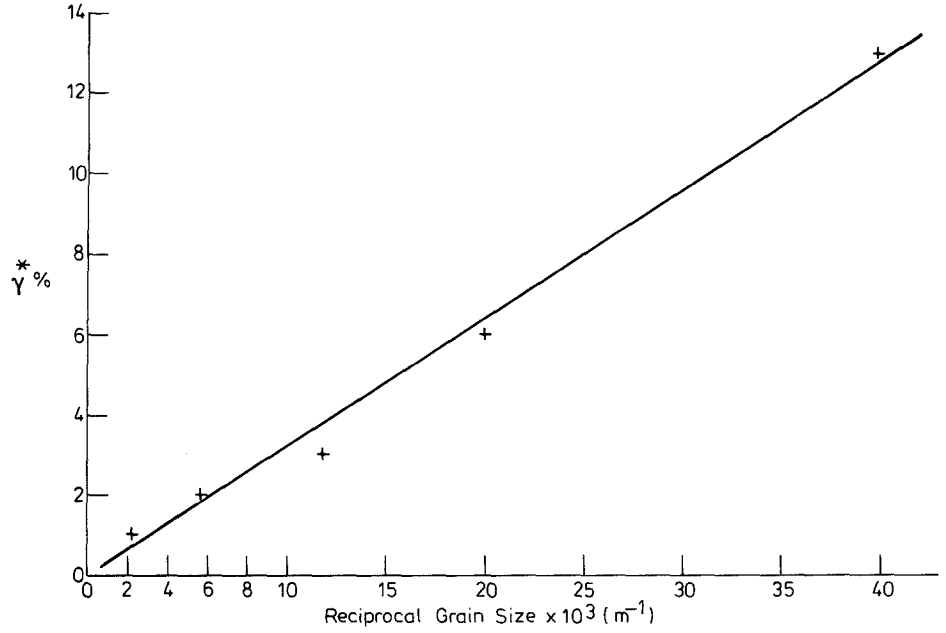

Figure 12 The ratio of grain-boundary to total strain (γ^*) as a function of reciprocal grain size.

Langdon [11] and observed experimentally by Lagneborg and Attermo [12].

In the following sections it has been assumed that γ^* has a constant value for each grain size and applied stress and is independent of strain up to nucleation; i.e. 0 to 20%. This may not be an entirely justifiable assumption in the present case where precipitation and re-orientation of grain boundaries occurs during creep testing but should not greatly affect the arguments. Using the stress dependency of grain-boundary sliding [10] it is possible to determine the extent of grain-boundary sliding in any of the specimens examined.

4.2. Crack nucleation

As indicated in Fig. 8, nucleation of wedge cracks occurs at an approximately constant value of creep strain, 16 to 18%, for each of the grain sizes

TABLE III Determination of grain-boundary displacement at crack initiation.

Grain size (μm)	$\bar{u}$ at failure (μm)	Rupture strain (%)	$\bar{u}$ at 17% strain (μm)
25	2.2	68	0.55
50	1.8	61	0.50
85	1.3	51	0.46
175	1.4	37	0.64
450	1.5	34	0.69

examined on testing at a stress of $220\,\mathrm{MN\,m^{-2}}$. Using the grain-boundary sliding data, the grain-boundary displacement corresponding to the nucleation strain has been calculated, see Table III, and it is seen to be approximately constant at $0.55\,\mu$m. The observation that crack nucleation at a given applied stress occurs at the same grain-boundary displacement irrespective of grain size is in accordance with Equation 2, derived for the case of cleavage crack nucleation (namely $\sigma_s nb = \frac{3}{8}\pi^2\gamma$, taking $nb = \bar{u}$).

Taking $\sigma_s = \sigma_{\text{applied}}/4$ to allow for shear on grain-boundary planes at low angles to the applied stress direction, as observed experimentally, the Stroh criterion (Equation 2) gives a value for the effective surface energy for grain boundary fracture of about $9\,\mathrm{J\,m^{-2}}$, independent of grain size.

The energy required for grain boundary fracture in a brittle manner is given by:

$$2\gamma = 2\gamma_s - \gamma_{gb}$$

where γ_s is the surface energy and γ_{gb} is the grain-boundary energy.

Taking γ_s to be $3\,\mathrm{J\,m^{-2}}$ and γ_{gb} to $1\,\mathrm{J\,m^{-2}}$, [13] the change in surface energy on crack formation is $5\,\mathrm{J\,m^{-2}}$ corresponding to γ in Equation 2 of $2.5\,\mathrm{J\,m^{-2}}$. The difference between this value and the experimental value determined from crack nucleation is associated with plastic deformation occurring during nucleation. Extensive plastic deformation is normally associated with creep crack propagation and failure, and in such cases very high fracture energies (200 to $250\,\mathrm{J\,m^{-2}}$) are obtained [14, 15]. The similarity between the change in surface energy for grain boundary fracture ($2.5\,\mathrm{J\,m^{-2}}$) and the value deduced from the experimental results ($9\,\mathrm{J\,m^{-2}}$) consequently suggests that relatively little plastic work is associated with triple point crack nucleation. Most of the external work required to produce fracture in this material is consequently associated with plastic deformation inside the grain and not with the intergranular fracture process, *per se*.

It has been observed in the present study that initial wedge crack nucleation is facilitated when the angle between the sliding grain boundary and the crack plane is high ($\theta/2 \sim 70$ to 80°). In terms of the nucleation condition described by Equation 2, initial nucleation would be expected to occur for wedging boundaries oriented in the maximum shear stress direction ($\theta/2 = 45^\circ$) when both the shear stress and the grain-boundary displacement are maxima [16]. The discrepancy between the observations and this expected optimum arrangement is not fully understood although it may in part by explained by grain-boundary re-orientation during creep.

The observed rapid initial increase in crack density with strain, followed by a tendency to saturation may be explained in terms of geometrical factors which take into account the variation of grain boundary sliding and stress concentrations with orientation. Thus, initial nucleation occurs at the optimum boundary arrangement (crack plane normal to stress direction and wedging boundaries enclosing an angle θ of about 150°). Later nucleation occurs for geometrical arrangements slightly away from this optimum arrangement, as increases in stress or strain lead to satisfaction of the Stroh criterion for other orientations. At an even later stage, when all moderately suitable triple points have nucleated cracks, much larger increases in stress or strain are required for further nucleation of cracks at highly non-ideal triple points and a tendency for saturation occurs.

In terms of this model of crack nucleation it is easy to understand how the nucleation plots for different grain sized materials may be made to superimpose, as in Fig. 10. Such nucleation curves are standardized in terms of cracks/grain and ϵ/ϵ_{crit}, where ϵ_{crit} is the strain at which nucleation begins. Thus, below ϵ_{crit}, no cracks exist. At ϵ_{crit}, nucleation occurs, and the crack density increases very rapidly to a value of cracks/grain of about 0.1 at a strain of $\epsilon/\epsilon_{crit} = 2$. Thereafter saturation of the number of cracks per grain becomes evident. The expression cracks/grain continues to increase until failure intercedes. The crack density by this time has reached a value of approximately 0.2 cracks/grain.

The plots in Fig. 10 superimpose when crack density per grain is plotted against strain because

ϵ_{crit} is approximately constant (17%) for each grain size examined. However, ϵ_{crit} has a value of about 35% for the two higher stresses investigated and it is necessary to re-plot the data using ϵ/ϵ_{crit}, for which case the crack density–normalized strain plots virtually superimpose for the four stresses examined as shown in inset of Fig. 11. Note that in this case it is sufficient to plot the crack density as cracks mm^{-2} to achieve the superposition because the grain size is the same for each test.

Using the same nucleation criterion as before (Equation 2 and the same value of surface energy, the grain boundary displacements corresponding to nucleation at 200, 290 and 330 $MN\,m^{-2}$ have been calculated (0.60, 0.35 and 0.29 μm). After creep strains of 17 and 35% these displacements correspond to values of γ^* of 6.7, 2 and 1.6% in reasonable accord with values obtained using the grain size and stress dependencies [10] of grain boundary sliding (7.2, 3.2 and 1.5%).

4.3. Nucleation away from triple points

Cavity or crack nucleation during creep often occurs at sites other than triple points, for example at grain boundary ledges or particles. Harris [5] has derived expressions which suggest that crack nucleation at grain-boundary particles as a result of grain-boundary sliding may be possible only at a late stage in the present tests when sufficiently large carbide or intermetallic particles have been produced. Subsequent cavity growth is limited by the extent of grain boundary sliding since diffusive growth requires much longer times at a temperature of 625° C with the result that such particle- or ledge-nucleated cavities, if formed, will only achieve very small sizes before failure has occurred by crack propagation.

4.4. Wedge crack growth

At 220 $MN\,m^{-2}$, wedge crack nucleation begins when the grain-boundary displacement reaches a value of 0.55 μm. Examining such crack nuclei in terms of an instability criterion for crack growth [17, 18] (namely $\sigma na = \sigma\bar{u} > 2\gamma$) it follows that if the effective surface energy γ retains the same value as at nucleation, such cracks should be unstable and propagate completely across their grain boundary facets. It is necessary to increase the effective surface energy to a value in excess of 70 $J\,m^{-2}$ to halt a crack before it reaches the other end of the facet and such cracks are in fact seen at all stages of the creep tests. This is an indication that extensive plastic deformation is associated with crack propagation across grain-boundary facets. It may be significant that cracks observed in materials strained slightly in excess of ϵ_{crit} are relatively large (typically in excess of 10 μm), whereas much smaller cracks (less than 5 μm) can be seen in specimens taken to fracture. This may be evidence of an increase in the effective surface energy with creep strain (or time) or, expressed in terms of the modified model of crack growth suggested by Heald and Williams [19], an increase in the size of the plastic zone of the crack as creep progresses.

5. Conclusions

(i) Wedge crack nucleation at 625° C and 220 $MN\,m^{-2}$, for the wide range of grain sizes examined (25 to 450 μm) occurs at a creep strain of approximately 17%, corresponding to a grain boundary displacement of 0.55 μm.

(ii) The condition for nucleation may be expressed in terms of the Stroh criterion for cleavage crack nucleation, namely $\sigma nb = 3\pi^2\gamma/8$, in which case the energy value determined, 9 $J\,m^{-2}$, is close to the free energy value. This low value of γ suggests that little grain boundary deformation is associated with nucleation and that only limited stress relaxation occurs during nucleation.

(iii) Nucleation of wedge cracks at other creep stresses may also be described by this expression using the same value for effective surface energy.

(iv) The first cracks to form are nucleated at the most suitable grain boundary triple point arrangements, namely crack plane perpendicular to the stress direction and sliding grain boundaries inclined at 60 to 80° to the crack plane. Subsequent nucleation occurs for geometrical arrangements slightly away from this ideal.

(v) Crack density–creep strain plots may be normalised in terms of cracks/grain and strain/critical strain, where the critical strain is that required for initial nucleation. Such normalised plots superimpose for creep carried out at different stresses using materials of different grain sizes.

References

1. G. W. GREENWOOD, Proceedings of the International Conference on Interfaces, Melbourne, 1969, p. 223.

2. A. N. STROH, *Proc. Roy. Soc.* **A 223** (1954) 404.
3. *Idem, Adv. Phys.* **6** (1957) 418.
4. E. SMITH, *Acta Met.* **14** (1966) 985.
5. J. E. HARRIS, *Trans. Met. Soc. AIME* **233** 1965 1509.
6. D. McLEAN, *J. Inst. Metals,* **11** (1956) 468.
7. J. S. WADDINGTON, *Phil. Mag.* **17** (1968) 145.
8. R. S. GATES and R. N. STEVENS, *Met. Trans.* **5** (1974) 505.
9. F. GARAFALO, W. F. DOMIS and F. VON GEMMINGEN, *Trans. Met. Soc. AIME* **230** (1964) 1460.
10. F. GARAFALO, O. RICHMOND, W. F. DOMIS and F. VON GEMMINGEN, *Proc. Inst. Mech. Eng.* **178** (1963) 1.
11. T. G. LANGDON, *Phil. Mag.* **22** (1970) 689.
12. R. LAGNEBORG and R. A. ATTERMO, *J. Mater. Sci.* **4** (1969) 195.
13. T. A. ROTH, *Mat. Sci. Eng.* **18** (1975) 183.
14. R. SODERBERG, *Met. Sci.* **9** (1975) 275.
15. J. A. WILLIAMS, *Acta Met.* **15** (1967) 1559.
16. R. C. GIFKINS, A. GITTUS, R. L. BELL and T. G. LANGDON, *J. Mater. Sci.* **3** (1968) 306.
17. J. A. WILLIAMS, *Phil. Mag.* **15** (1967) 1289.
18. A. H. COTTRELL, *Trans. Met. Soc. AIME* **212** (1958) 192.
19. P. T. HEALD and J. A. WILLIAMS, *Phil. Mag.* **22** (1970) 1095.

Received 17 November 1976 and accepted 26 January 1977.